Autler–Townes Splitting in a Δ-Type Quantum Three-Level System *

Qi-Chun Liu(刘其春), Han Cai(蔡涵), Ying-Shan Zhang(张颖珊), Jian-She Liu(刘建设), Wei Chen(陈炜)**

Institute of Microelectronics, Department of Microelectronics and Nanoelectronics and Tsinghua National Laboratory of Information Science and Technology, Tsinghua University, Beijing 100084

(Received 26 February 2016)

We observe the Autler–Townes splitting effect in a Δ-type quantum three-level system, using the lowest three levels of a SQUID-type Al/AlOx/Al transmon qubit embedded in a three-dimensional copper microwave cavity. A control tone at different strengths is applied in resonance with the transition between the first and second excited states, while the spectra between each of them and the ground state are probed by another microwave tone. The experimental result shows the difference between the two spectra, and fits well with the Lindblad master equation model.

PACS: 42.50.Ct, 32.80.Qk, 74.78.Na DOI: 10.1088/0256-307X/33/7/074205

As an artificial atom, a superconducting quantum circuit exhibits its great potential in implementing quantum computation and on-chip quantum optics experiments.[1] One of these impressive quantum optics effects is the Autler–Townes splitting (ATS),[2] which happens when we drive a quantum three-level system with a strong drive field, resonant with two of the levels. It is caused by the electromagnetic pumping doublet structure. ATS is closely related to another kind of quantum optics effect, called electromagnetically induced transparency (EIT),[3,4] which is caused by destructive interference between two different excitation pathways. Both ATS and EIT effects create a transparency window in the absorption or transmission spectrum. These two kinds of quantum optics effects have been studied variously in superconducting quantum circuit systems,[5–18] and to distinguish ATS and EIT effects, some methods have been reported.[19–22]

In all the reported ATS experiments, realized in the superconducting circuit quantum electrodynamic (QED) systems, the three-level system is only taken as Ξ-type, corresponding to the quantum system working at the optimal point. One-photon transition process between the ground state and the second excited state is forbidden at the optimal point,[23] thus only the spectrum of transition between the ground and first excited states is probed.

However, in some superconducting circuit QED systems, taking transmon for an example, the charge bias $n_{\rm g}$ is not set at 0.5, which means that the qubit is no longer set at the optimal point anymore. Thus one-photon transition process between the ground and second excited states is not forbidden and must be taken into account. For further studying of the ATS effect in a superconducting quantum circuit, we take the three-level system as a Δ-type (see Fig. 1(b)), with a control tone resonant with the transition between the second and first excited states. By probing both levels subjected to the control tone, we can compare the splitting effect of the two levels. Our experimental result can be well explained by the model of a three-level system with a control and a probe fields.

The device, used for our experiment in this study, is a tunable 3D transmon,[24,25] whose single Josephson junction is replaced by a superconducting quantum interference device (SQUID) with two junctions. The transmon is fabricated on the silicon dioxide substrate with a standard double-angle evaporation process; the Al/AlOx/Al junction[26] has an area of $100\,{\rm nm}\times 250\,{\rm nm}$, the SQUID loop is of the size $2.5\,\mu{\rm m}\times 3.5\,\mu{\rm m}$ and each Al shunting capacitor pad has an area of $250\,\mu{\rm m}\times 500\,\mu{\rm m}$. The transmon is embedded in a 3D copper microwave cavity,[27] with a global magnetic bias which can tune the effective Josephson energy of the transmon. Our experiment was performed in a dilution refrigerator at base temperature 20 mK.

In the experiment reported here, the effective Josephson energy $E_{\rm J}$ and the charging energy $E_{\rm C}$ are measured to be $E_{\rm J}/h = 15.000\,{\rm GHz}$ and $E_{\rm C}/h = 345\,{\rm MHz}$. The first mode bare frequency of cavity is 8.1920 GHz with a loaded quality factor $Q_{\rm L} \sim 8000$. The state of the transmon, representing the absorption of the probe field, is revealed by the cavity transmission at dispersive frequency ($\omega_{\rm cavity} = 2\pi\times 8.2029\,{\rm GHz}$), and the transmission of the cavity is measured by a parameter network analyzer with power $-70\,{\rm dBm}$ at the source output. Taking into account an attenuation of $-80\,{\rm dB}$ before cavity, $-70\,{\rm dBm}$ corresponds to 0.2 average photons in the cavity.

We denote the lowest three levels of transmon as

*Supported by the National Basic Research Program of China under Grant Nos 2011CBA00304, 2014CB848700 and 2014CB921401.

**Corresponding author. Email: weichen@tsinghua.edu.cn

© 2016 Chinese Physical Society and IOP Publishing Ltd

$|i\rangle$ ($i = 0$, 1 and 2), with the corresponding eigenenergy $\hbar\omega_i$ and the transition frequency between states $|i\rangle$ and $|j\rangle$ being $\omega_{ij} = \omega_i - \omega_j$ ($i > j$) (see Fig. 1(b)). We obtain the spectrum of the qubit by applying a probe tone with frequency around ω_{10} (ω_{20}) and measure the transmission of cavity in dispersive regime. By fitting the spectrum with a Lorentzian, we obtain the damping rates $\gamma_{10} = 2\pi \times 1.74\,\mathrm{MHz}$ and $\gamma_{20} = 2\pi \times 4.02\,\mathrm{MHz}$, as well as the corresponding transition frequencies $\omega_{10} = 2\pi \times 6.0893\,\mathrm{GHz}$ and $\omega_{20} = 2\pi \times 11.8336\,\mathrm{GHz}$.

In the experiment, the three-level system is driven with a control tone, resonant with the transition frequency between $|2\rangle$ and $|1\rangle$ ($\omega_c = \omega_{21}$), and a probe tone, slightly detuned from the transition frequency between $|n\rangle$ and $|0\rangle$ ($\omega_p^{n0} = \omega_{n0} - \delta_{n0}$, $n = 1$ and 2). The corresponding strengths are Ω_c and Ω_p^{10} (Ω_p^{20}), respectively.

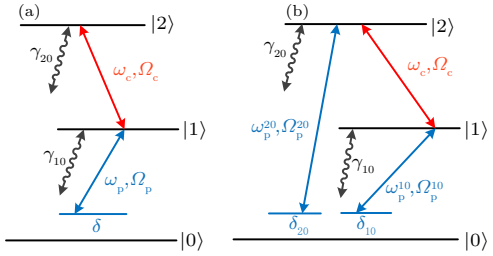

Fig. 1. (a) The Ξ-type three-level system. One photon transition process between the ground and second excited states is forbidden. (b) The Δ-type three-level system. It is driven with a control tone resonant with the transition between $|2\rangle$ and $|1\rangle$, and the probe tone with frequency ω_p^{10} (ω_p^{20}) having a detuning δ_{10} (δ_{20}) from the transition between $|1\rangle$ ($|2\rangle$) and $|0\rangle$. The strengths are Ω_c and Ω_p^{10} (Ω_p^{20}), respectively.

Another measurement tone is applied in resonance with the dispersive frequency of the cavity when the transmon is in the ground state $|0\rangle$, and the strength is Ω_m. Under the rotating-wave approximation, the system Hamiltonian is $H^n = H_0^n + H_{\mathrm{int}}^n$, with

$$\begin{aligned} H_0^n =& \hbar\delta_{n0}(\sigma_{22} + \sigma_{11}) - \hbar[\Omega_p^{n0}(\sigma_{n0} + \sigma_{0n}) \\ &+ \Omega_c(\sigma_{21} + \sigma_{12}) + \Omega_m a^\dagger a], \\ H_{\mathrm{int}}^n =& -\Big[\frac{g^2}{\Delta_{10}}\sigma_{00} + \Big(\frac{g^2}{\Delta_{10}} - \frac{2g^2}{\Delta_{21}}\Big)\sigma_{11} \\ &+ \frac{2g^2}{\Delta_{21}}\sigma_{22}\Big]a^\dagger a, \end{aligned} \tag{1}$$

where $\sigma_{ij} = |i\rangle\langle j|$ is the atomic projection operator, a ($a^\dagger$) is the annihilation (creation) operator of the cavity mode, g is the coupling strength between the cavity and the transition $|0\rangle \leftrightarrow |1\rangle$, $\Delta_{ij} = \omega_{ij} - \omega_{\mathrm{cavity}}$, H_0^n describes that the three-level system is driven with the control and probe tones while the cavity is measured by a measurement tone, and H_{int}^n represents the interaction between the three-level system and the cavity. The quantum dynamics of the system can be described by a Lindblad master equation

$$\frac{d\rho}{dt} = -\frac{i}{\hbar}[H^n, \rho] + \mathcal{L}[\rho], \tag{2}$$

with the Lindblad term

$$\begin{aligned} \mathcal{L}[\rho] =& \Gamma_{21}\rho_{22}(-\sigma_{22} + \sigma_{11}) + \Gamma_{10}\rho_{11}(-\sigma_{11} + \sigma_{00}) \\ &+ \Gamma_{20}\rho_{22}(-\sigma_{22} + \sigma_{00}) - \sum_{i\neq j}\gamma_{ij}\rho_{ji}\sigma_{ij} \\ &+ \frac{\kappa}{2}\mathcal{D}[a]\rho, \end{aligned} \tag{3}$$

where γ_{ij} ($=\gamma_{ji}$) and Γ_{ij} ($i > j$, $i, j = 0$, 1 and 2) are the damping rate and relaxation rate between state $|i\rangle$ and $|j\rangle$, ρ is the system density matrix $\rho = \rho_{ij}|i\rangle\langle j|$, and $\mathcal{D}[a]\rho = 2a\rho a^\dagger - a^\dagger a\rho - \rho a^\dagger a$ denotes the decay rate of the cavity photon levels.

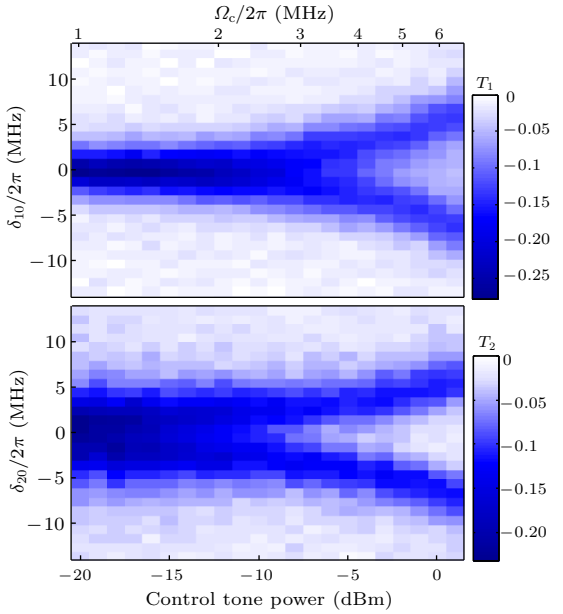

Fig. 2. The spectrum T_1 (T_2) of transition between $|1\rangle$ ($|2\rangle$) and $|0\rangle$. The control tone power increases from -20 dBm to 1 dBm at source output and it is resonant with the transmon transition frequency ω_{21}. The probe tone has a detuning δ_{10} (δ_{20}) from transition frequency ω_{10} (ω_{20}) and the strength is about 0.5 MHz, extracted from the time domain Rabi oscillation measurement.

When the probed level is $|n\rangle$ ($n = 1$ and 2), the cavity transmission T_n, obtained by the cavity measurement tone, is proportional to the average photons $\langle a^\dagger a\rangle$ in the cavity, and depends on the occupation probability of the transmon being in each state. It is given by $T_n = \rho_{00}T_0' + \rho_{11}T_1' + \rho_{22}T_2'$, where $\rho_{00} + \rho_{11} + \rho_{22} = 1$ and T_0', T_1' and T_2' are the cavity transmission when the qubit is in $|0\rangle$, $|1\rangle$ and $|2\rangle$ states, respectively. In this work, T_0' is normalized to 0 and $r_T \equiv T_1'/T_2'$, thus $T_n \equiv \rho_{22} + r_T\rho_{11})|_n$. For a weak probe field ($\Omega_p^{n0} \ll \gamma_{10}, \gamma_{20}$), starting from the ground state, solving the master Eq. (2) in a steady state gives

a good approximate solution for $(\rho_{22}+r_T\rho_{11})|_n$,

$$T_1 \equiv (\rho_{22}+r_T\rho_{11})|_{n=1} = \frac{A_1\Omega_{\rm p}^{10}\left(\gamma_{10}+\frac{\Omega_{\rm c}^2\gamma_{20}}{\delta_{10}^2+\gamma_{20}^2}\right)}{\left(\delta_{10}-\frac{\Omega_{\rm c}^2\delta_{10}}{\delta_{10}^2+\gamma_{20}^2}\right)^2+\left(\gamma_{10}+\frac{\Omega_{\rm c}^2\gamma_{20}}{\delta_{10}^2+\gamma_{20}^2}\right)^2}, \quad (4)$$

$$T_2 \equiv (\rho_{22}+r_T\rho_{11})|_{n=2} = \frac{A_2\Omega_{\rm p}^{20}\left(\gamma_{20}+\frac{\Omega_{\rm c}^2\gamma_{10}}{\delta_{20}^2+\gamma_{10}^2}\right)}{\left(\delta_{20}-\frac{\Omega_{\rm c}^2\delta_{20}}{\delta_{20}^2+\gamma_{10}^2}\right)^2+\left(\gamma_{20}+\frac{\Omega_{\rm c}^2\gamma_{10}}{\delta_{20}^2+\gamma_{10}^2}\right)^2}. \quad (5)$$

In Fig. 2 we show T_1 and T_2 for different control tone powers, ranging from -20 dBm to 1 dBm at the source output. The top one shows the spectrum with state $|1\rangle$ being probed, while the bottom one shows the spectrum with state $|2\rangle$ being probed. By fitting T_1 and T_2 with Eqs. (4) and (5) respectively, we can obtain the control tone strength $\Omega_{\rm c}$. For example, Fig. 3 shows the fitting of experimental data T_1 and T_2 at some typical control tone powers: -15 dBm, -10 dBm, -5 dBm and 0 dBm (corresponding to the control tone strengths $\Omega_{\rm c}/2\pi$ being 1.37, 2.14, 3.52 and 6.01 MHz, respectively). We can see that all the experimental results can be well described by Eqs. (4) and (5) with $\gamma_{10}=2\pi\times1.74$ MHz, $\gamma_{20}=2\pi\times4.02$ MHz and two fitting parameters $\Omega_{\rm c}$ and $A_1\Omega_{\rm p}^{10}$ ($A_2\Omega_{\rm p}^{20}$).

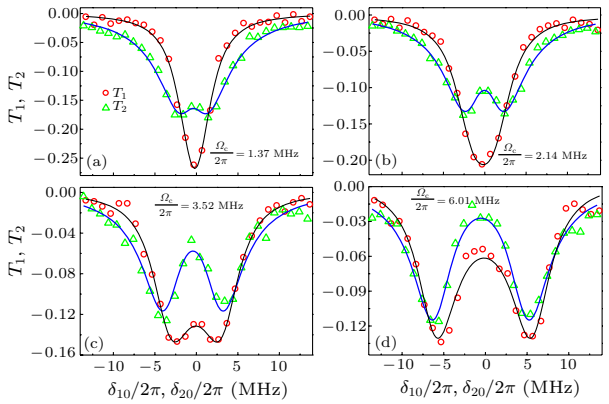

Fig. 3. The fitting of T_1 denoted by red circle, (T_2 denoted by green triangle) with Eq. (4) (Eq. (5)) with fitting parameters $\Omega_{\rm c}$ and $A_1\Omega_{\rm p}^{10}$ ($A_2\Omega_{\rm p}^{20}$) at some typical control tone powers: -15 dBm, -10 dBm, -5 dBm and 0 dBm, from (a) to (d). The solid curves, black for T_1 and blue for T_2, are the fitting results with $\Omega_{\rm c}/2\pi = 1.37$, 2.14, 3.52 and 6.01 MHz.

Due to the fact that states $|1\rangle$ and $|2\rangle$ are subjected to the same control tone field, the spectrum T_1 should give the same control strength as that given by spectrum T_2, for the same control tone power. In Fig. 4(a), the red open circles (green open triangles) represent the control strengths for different control tone amplitudes obtained by fitting T_1 (T_2) with Eq. (4) (Eq. (5)), while the black (blue) solid line is a linear fit. The control strength obtained by T_1 is the same as that given by T_2, considering the experiment error of about 4%, although spectrum T_1 is totally different from spectrum T_2. At the same time, the linearity of control strength with control tone amplitude shows that the system fits well with the theory of a two-level system with a resonant drive.

For the ATS effect, one usually considers the splitting space of the doublet spectrum as twice as the control strength. This is a good approximation for a sufficiently strong control field, while for the condition where the control strength is comparable with the damping rates of the system, one cannot use this approximation anymore. Here we take the frequency space between the two minimum points of spectrum T_1 (T_2) as the splitting space of the doublet. If there is only one minimum point, the splitting space is taken as 0. In Fig. 4(b), we show the splitting space of experimental results. Red circles (green triangles) indicate the result of T_1 (T_2).

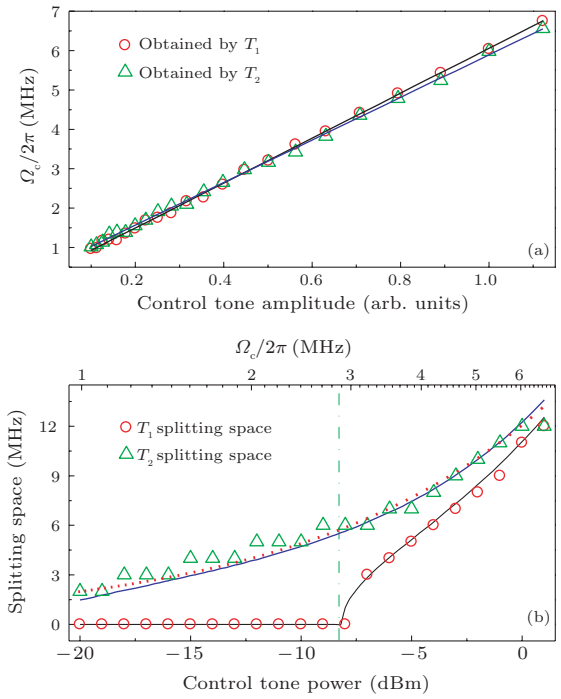

Fig. 4. (a) Control tone strength at different control field amplitudes obtained by fitting T_1 (T_2) with Eq. (4) (Eq. (5)), indicated by red circles (green triangles), while the black (blue) solid line is a linear fitting. (b) The splitting space of the spectrum at different control tone strengths. Red circles (green triangles) represent the results of T_1 (T_2). The black (blue) solid line is calculated by $d{\rm Im}(\rho_{10})/d\delta_{10}=0$ ($d{\rm Im}(\rho_{20})/d\delta_{20}=0$), while the red dotted line indicates that the splitting is twice the control tone strength. The green dashed-dotted line indicates that $\Omega_{\rm c}=(\gamma_{10}+\gamma_{20})/2=2\pi\times2.88$ MHz.

By solving $d{\rm Im}(\rho_{10})/d\delta_{10}=0$ ($d{\rm Im}(\rho_{20})/d\delta_{20}=0$), with $\gamma_{10}/2\pi=1.74$ MHz and $\gamma_{20}/2\pi=4.02$ MHz, the theoretical splitting space of T_1 (T_2) for different control strengths (i.e., different drive field powers) can be obtained, as shown by the black (blue) solid line in Fig. 4(b). We can see that the experimental result fits

well with the theoretical calculation. When the control tone is strong enough ($\Omega_c \gg \gamma_{10}, \gamma_{20}$), the splitting space is almost twice the control strength. When the control tone is slightly weak ($\Omega_c < (\gamma_{10} + \gamma_{20})/2$), the splitting spaces of spectra T_1 and T_2 are totally different. No doublet is shown in T_1 while the splitting of spectrum T_2 is significant in this regime. In fact, under this condition the spectrum T_2 of the system is already in the transition regime between ATS and EIT effects. The two extreme points in T_2 are no longer only caused by dynamic shift. The EIT effect also has an effect on it. In our other system with the same experimental setup, by adjusting the damping rates, the system can fulfill the condition for realizing EIT and exhibits a clear EIT effect.

In summary, we have measured the ATS effect in a Δ-type 3D transmon superconducting system. A control tone is applied in resonance with the transition between the first and second excited states, and the transition spectra between each of them and the ground state have been probed. The experiment is well described by the model of a three-level system with two drive tones. Further analysis and comparison show that though the first and second excited states are subject to the same control tone, the splitting of the spectra are different. This gives a more complete dressed-state spectrum of the three-level system and it can be used to control two microwave tones at the same time with one control field.

References

[1] You J Q and Nori F 2011 *Nature* **474** 589
[2] Aulter S H and Townes C H 1955 *Phys. Rev.* **100** 703
[3] Fleischhauer M, Imamoglu A and Marangos J P 2005 *Rev. Mod. Phys.* **77** 633
[4] Marangos J P 1998 *J. Mod. Opt.* **45** 471
[5] Xu H K, Song C, Liu W Y, Xue G M, Su F F, Deng H, Tian Ye, Zheng D N, Han Siyuan, Zhong Y P, Wang H, Liu Y X and Zhao S P 2016 *Nat. Commun.* **7** 11018
[6] Kumar K S, Vepsäläinen A, Danilin S and Paraoanu G S 2016 *Nat. Commun.* **7** 10628
[7] Novikov S, Sweeney T, Robinson J E, Premaratne S P, Suri B and Wellstood F C 2015 *Nat. Phys.* **12** 75
[8] Cho S U, Moon H S, Chough Y T, Bae M H and Kim N 2014 *Phys. Rev.* A **89** 053814
[9] Wang H, Gu X, Liu Y X, Miranowicz A and Nori F 2014 *Phys. Rev.* A **90** 023817
[10] Novikov S, Robinson J E, Keane Z K, Suri B, Wellstood F C and Palmer B S 2013 *Phys. Rev.* B **88** 060503(R)
[11] Suri B, Keane Z K and Ruskov R 2013 *New J. Phys.* **15** 125007
[12] Hoi I C, Wilson C M, Johansson G, Palomaki T, Peropadre B and Delsing P 2011 *Phys. Rev. Lett.* **107** 073601
[13] Li J, Paraoanu G S, Cicak K, Altomare F, Park J I, Simmonds R W, Sillanpää M A and Hakonen P J 2011 *Phys. Rev.* B **84** 104527
[14] Kelly W R, Dutton Z, Schlafer J, Mookerji B, Ohki T A, Kline J S and Pappas D P 2010 *Phys. Rev. Lett.* **104** 163601
[15] Abdumalikov A A, Astafiev O, Zagoskin A M, Pashkin Yu A, Nakamura Y and Tsai J S 2010 *Phys. Rev. Lett.* **104** 193601
[16] Ian H, Liu Y X and Nori F 2010 *Phys. Rev.* A **81** 063823
[17] Sillanpää M A, Li J, Cicak K, Altomare F, Park J I, Simmonds R W, Paraoanu G S and Hakonen P J 2009 *Phys. Rev. Lett.* **103** 193601
[18] Baur M, Filipp S, Bianchetti R, Fink J M, Göppl M, Steffen L, Leek P J, Blais A and Wallraff A 2009 *Phys. Rev. Lett.* **102** 243602
[19] Lu X G, Miao X X, Bai J H, Pei L Y, Wang M, Gao Y L, Wu L A, Fu P M, Wang R Q and Zuo Z C 2015 *J. Phys. B: At. Mol. Opt. Phys.* **48** 055003
[20] Sun H C, Liu Y X, Ian H, You J Q, Ilichev E and Nori F 2014 *Phys. Rev.* A **89** 063822
[21] Peng B, Özdemir S K, Chen W J, Nori F and Yang L 2014 *Nat. Commun.* **5** 5082
[22] Anisimov P M, Dowling J P and Sanders B C 2011 *Phys. Rev. Lett.* **107** 163604
[23] Liu Y X, You J Q, Wei L F, Sun C P and Nori F 2005 *Phys. Rev. Lett.* **95** 087001
[24] Rigetti C, Gambetta J M, Poletto S, Plourde B L T, Chow J M, Córcoles A D, Smolin J A, Merkel S T, Rozen J R, Keefe G A, Rothwell M B, Ketchen M B and Steffen M 2012 *Phys. Rev.* B **86** 100506(R)
[25] Paik H, Schuster D I, Bishop L S, Kirchmair G, Catelani G, Sears A P, Johnson B R, Reagor M J, Frunzio L, Glazman L I, Girvin S M, Devoret M H and Schoelkopf R J 2011 *Phys. Rev. Lett.* **107** 240501
[26] Wu Y L, Deng H, Yu H F, Xue G M, Tian Y, Li J, Chen Y F, Zhao S P and Zheng D N 2013 *Chin. Phys.* B **22** 060309
[27] Zhao H, Li T F, Liu Q C, Liu J S and Chen W 2014 *Chin. Phys. Lett.* **31** 102101